Computational Study on the Interaction Between a Vortex and a Shock Wave

Kristine R. Meadows,* Ajay Kumar,† and M.Y. Hussaini‡
NASA Langley Research Center, Hampton, Virginia

A computational study of two-dimensional shock vortex interaction is discussed in this paper. A second-order upwind finite volume method is used to solve the Euler equations in conservation form. In this method, the shock wave is captured rather than fitted so that the cases where shock vortex interaction may cause secondary shocks can also be investigated. The effects of vortex strength on the computed flow and acoustic field generated by the interaction are qualitatively evaluated.

Introduction

THE development of a numerical method for predicting sound waves generated by shock vortex interaction has a variety of potential applications in the design of supersonic and subsonic aircraft. Advanced design jet engines may operate at supercritical nozzle pressure ratios, resulting in the development of a shock structure in the jet plume. Turbulent eddies in the jet interact with the shock structure creating "shock associated jet noise" or "shock noise."[1,2] Broadband shock noise is an important factor in the design of advanced jet engines because of the effect on community noise, aircraft interior noise, and structural fatigue. Similarly, in the case of helicopter blades operating at supercritical speeds, a shock may form on the blade surface and the trailing vortices from a preceding blade may interact with this shock resulting in impulsive noise. Yet another application of the study of shock vortex interaction is in the investigation of turbulence amplification by the shock in a variety of flows. Hence, the knowledge gained by an understanding of the physics of the shock-vortex interaction process has application to real aerodynamic problems.

Early studies of shock-vortex interaction focused primarily on the development of predictive linear theories that were compared with experimental results.[3-12] In this decade, however, investigators have mainly concentrated on numerical methods for analyzing the problem. In 1981, Pao and Salas[13] performed a numerical analysis of shock-vortex interaction by using a MacCormack finite-difference method to solve the Euler equations. Salas, Zang, and Hussaini,[14] Hussaini et al.,[15] and Kopriva et al.[16] applied spectral methods to the same problem. One major disadvantage of the approaches used in these numerical solutions is that the physical domain continually grows with time, thereby decreasing the accuracy of the solution as one progresses temporally.

Recently, Kopriva[17] applied a multidomain spectral approach to avoid the loss of accuracy resulting from grid expansion. However, even though Kopriva's method may have improved the resolution of this problem, there is yet another disadvantage of the preceding numerical techniques in that they all use shock fitting with Rankine-Hugoniot relations across the shock. This limits the application of the methods to only weak interactions where the shock is deformed only slightly. In cases of strong interactions, where the shock deforms significantly and may even produce secondary shocks, shock-fitting techniques are difficult to apply. Linear theory is also not applicable in such cases. Further, the preceding techniques are difficult to apply to realistic two- and three-dimensional geometries. It is, therefore, necessary to investigate new techniques where such restrictions can be avoided.

The computational procedure investigated in this paper solves the nonlinear Euler equations in conservation form by an upwind method, so that the shock is captured as part of the fluid dynamic solution. This is advantageous because it avoids the difficulties of applying the shock-fitting technique to the cases where the shock-vortex interaction is strong enough to cause the shock to branch into several shocks. Furthermore, extension of shock capturing methods to the more practical case of three-dimensional interactions is straightforward.

Problem Formulation

The first step in formulating the shock-vortex interaction problem in the present study is to establish a flowfield with a stable normal shock. This is accomplished by introducing supersonic Mach 1.1 flow at the inlet of a slightly diverging duct, shown schematically in Fig. 1. Slight divergence of half a degree is required to stabilize the shock in the duct. A back pressure ratio of 1.339 is chosen so that the normal shock is established approximately at the middle of the duct length. After this initial steady-state flowfield is established with a normal shock in the duct, a vortex is superimposed on the flow upstream of the shock and is allowed to propagate with the flow through the shock to the duct outlet.

The Euler equations are selected to be the appropriate governing equations for the flow, since the viscous effects are assumed to be negligible away from the walls. These equations can be written in conservation form as

$$\frac{\partial \hat{Q}}{\partial t} + \frac{\partial \hat{F}}{\partial \xi} + \frac{\partial \hat{G}}{\partial \eta} = 0 \tag{1}$$

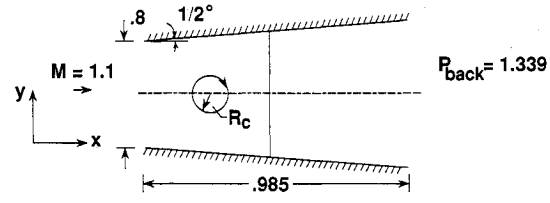

Fig. 1 Model Problem. Vortex Core R_c = .075. Pressure ratio across shock, ΔP_s = 1.28.

Received July 18, 1989; revision received Jan. 2, 1990.

*Aerospace Engineer. Member AIAA.
† Head, Computational Methods Branch. Associate Fellow AIAA.
‡ Chief Scientist, Institute for Computer Applications in Science and Engineering (CASE). Associate Fellow AIAA.

The vectors in Eq. (1) are

$$\hat{Q} = \frac{Q}{J} = \frac{1}{J}\begin{Bmatrix} \rho \\ \rho u \\ \rho v \\ e \end{Bmatrix} \tag{2}$$

$$\hat{F} = \frac{1}{J}\begin{Bmatrix} \rho U \\ \rho U u + \rho \xi_x \\ \rho U v + \rho \xi_y \\ (e + \rho)U \end{Bmatrix} \tag{3}$$

$$\hat{G} = \frac{1}{J}\begin{Bmatrix} \rho V \\ \rho V u + \rho \eta_x \\ \rho V v + \rho \eta_y \\ (e + p)V \end{Bmatrix} \tag{4}$$

where

J = Jacobian of the transformation
ρ = density
ρU = momentum in ξ direction
ρV = momentum in η direction
e = total energy per unit volume
p = pressure
u = velocity in x direction
v = velocity in y direction

The equation of state for a perfect gas is

$$p = (\gamma - 1)[e - \rho(u^2 + v^2)/2] \tag{5}$$

where γ = ratio of specific heats = 1.4. The equations have been generalized from Cartesian coordinates using a transformation of the type

$$\xi = \xi(x,y) \quad \eta = \eta(x,y) \tag{6}$$

The contravariant velocity components are written

$$U = \xi_x u + \xi_y v \tag{7a}$$

$$V = \eta_x u + \eta_y v \tag{7b}$$

All thermodynamic variables are normalized with respect to the freestream conditions at the duct inlet. Lengths are normalized with a reference unit length, and velocities are normalized by the freestream speed of sound. Time is nondimensionalized by the freestream speed of sound and reference unit length. Tangency boundary conditions are applied at the duct walls. Thermodynamic properties are specified at the duct inlet. The back pressure at the duct outlet is fixed.

The governing equations are solved on a grid of 132 points in the axial direction and 122 grid points in the normal direction. The grid is refined in the axial direction around the shock, as illustrated in Fig. 2.

A second-order accurate upwind finite volume technique, based upon flux vector splitting, is used to solve the governing equations. This method unlike central difference methods, captures shocks more accurately with little or no pre- and postshock oscillations. One reason this particular method is interesting from an acoustic perspective is that it simulates signal propagation features of the hyperbolic equations. Therefore, the method is inherently capable of obtaining wave-type solutions of the fluid dynamic equations. A basic characteristic of the flux split upwind method is that the fluxes are split into forward and backward contributors according to the signs of the wave propagation. The details of the method and its implementation to solve the Euler equations are given in Refs. 18 and 19. Discussions of the dispersion and dissipation of the upwind method is given in Ref. 20.

Hybrid Vortex Model

The hybrid vortex models vortical flow as a mass rotating at constant velocity everywhere within the core and decaying exponentially outside the core. The velocity profile is

$$U_\theta(r) = U_c, \qquad r \le R_c \tag{8a}$$

$$U_\theta(r) = U_c \exp -(r^2 - R_c^2)/\Omega, \qquad r > R_c \tag{8b}$$

where

U_θ = tangential velocity
U_c = constant core velocity
r = distance from the vortex center
R_c = vortex core radius
Ω = vortex decay parameter

For the computations performed here, the core radius is 0.075, the vortex decay parameter is 0.0115, and the strength of the vortex, indicated by tangential velocity at the vortex core, is varied. A parametric study of vortex strength is performed, and the results for the tangential velocities at the vortex core, corresponding to the weak $U_c = 0.1$ and strong $U_c = 0.3$ vortices, are presented. This vortex model and the fixed parameters are selected so that the effect of the wall on the vortex is negligible. Specifically, the core radius is small compared to the channel width and the tangential velocity approaches zero at the channel walls. The vortex model is computationally convenient because the rapid decrease of velocity with increasing distance from the vortex center allows one to use a computational grid of small extent. The velocity profile for the hybrid vortex is illustrated in Fig. 3.

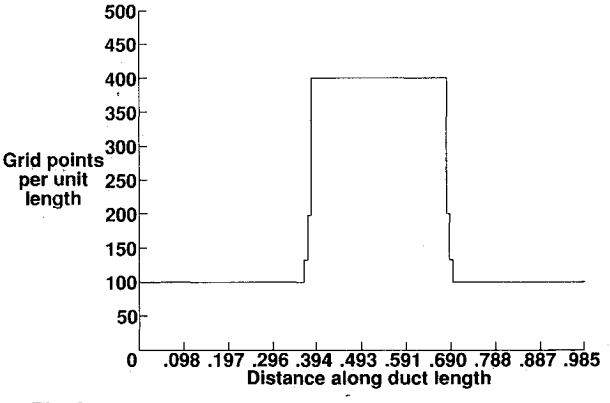

Fig. 2 Distribution of grid points along the duct length.

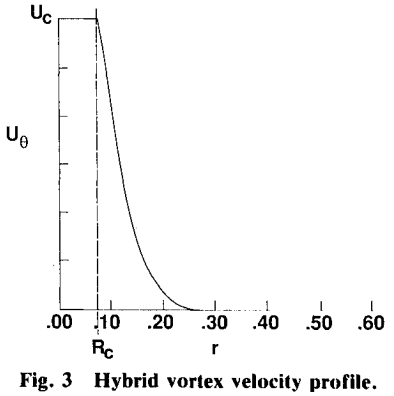

Fig. 3 Hybrid vortex velocity profile.

It should be noted here that several vortex models were used to evaluate the effect of vortex modeling on the solution. Since the results obtained with the vortex models were very similar, only the hybrid vortex model and its results have been discussed in this paper. The hybrid vortex was chosen over the classical vortex of constant angular velocity for computational considerations. The classical vortex does not decay rapidly enough to allow the assumption of negligible velocity at the wall. The number of grid points in the vertical direction must be decreased for the classical vortex, resulting in more computer run time.

Results

Figure 4 shows a time history of pressure contours for a weak $U_c = 0.1$ hybrid clockwise-rotating vortex interacting with a shock. Figure 4a, corresponding to a normalized time of 0.05 after the introduction of the vortex on the flow, shows the vortex approaching the shock. The flow upstream of the shock shows the circular pressure contour lines resulting from the presence of the vortex and expansion lines due to the slight divergence of the channel. The flow downstream of the shock is undisturbed. Figure 4b presents results at a normalized time of 0.15. The vortex core has not yet interacted with the shock, but the velocity field induced by the vortex is beginning to disturb the flow downstream of the shock. Figure 4c shows contours corresponding to a normalized time of 0.25. The vortex core has interacted with the shock at this time and two distinct pressure regions are seen to develop on the downstream side of the shock. The region above the vortex center is at a pressure higher than the steady-state condition, and the region below the vortex center is at a pressure lower than the steady-state condition. The regions of high and low pressure

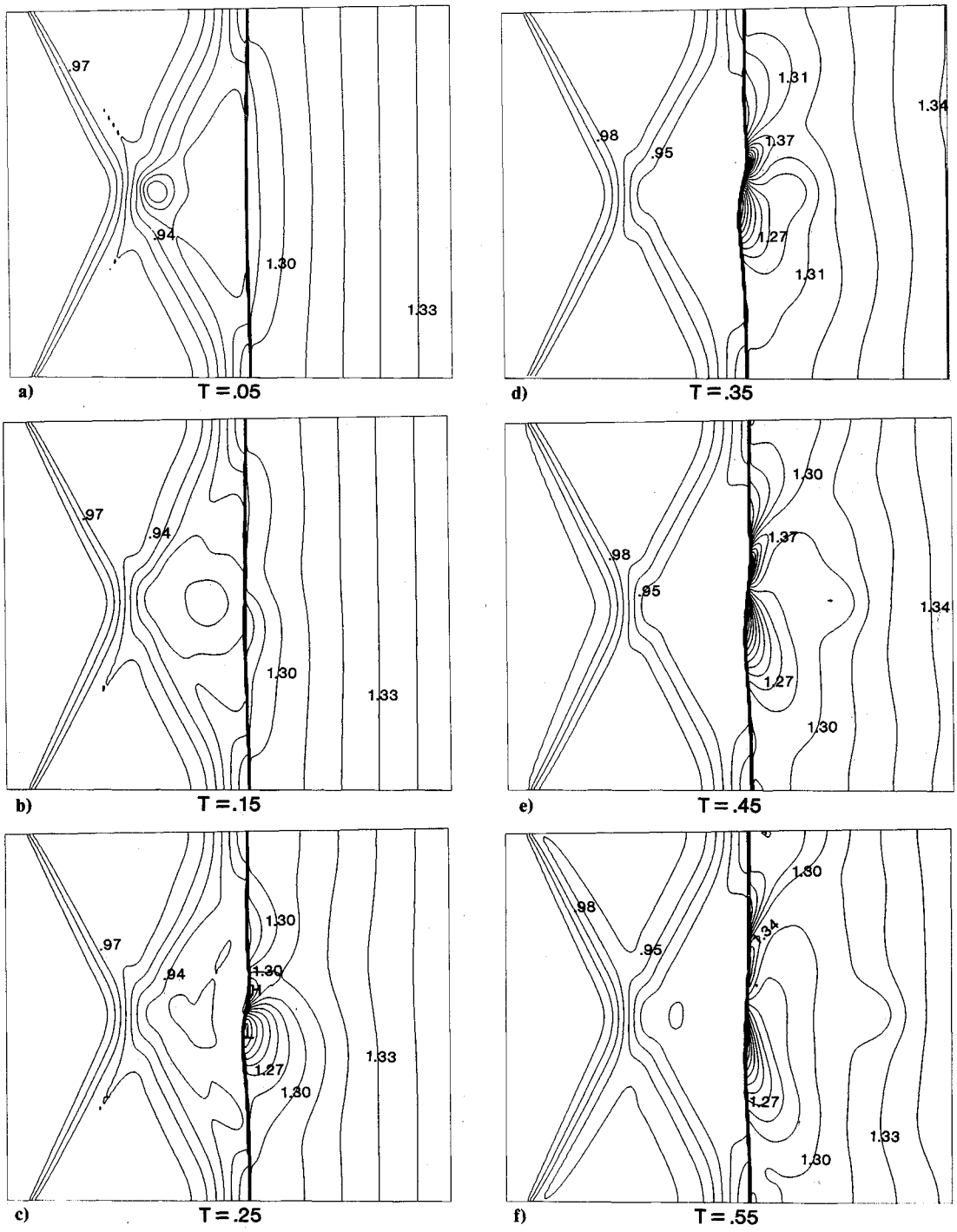

Fig. 4 Time history of pressure contours. Weak vortex ($U_c = 0.1$).

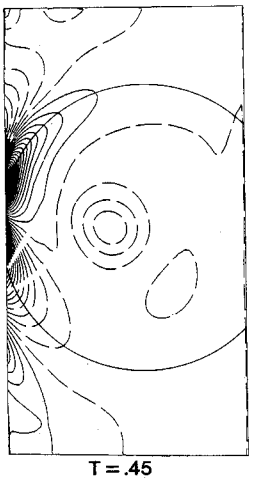

Fig. 5 Contours of change in pressure. Weak vortex ($U_c = 0.1$) at dimensionless time 0.45. Dashed lines represent loss in pressure from steady-state condition. Solid lines represent increase in pressure.

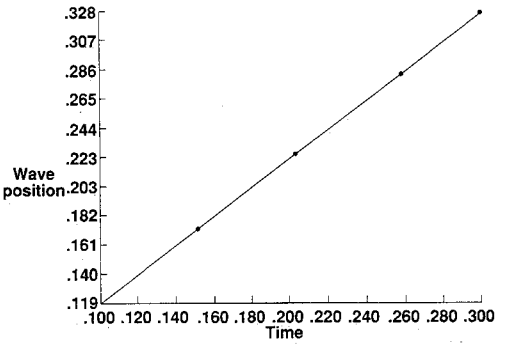

Fig. 6 Acoustic wavefront position as a function of normalized time.

are marked with an H and an L, respectively, on Fig. 4c. A wavefront centered on the vortex core is seen to develop in subsequent time steps. To more clearly see the development of this wavefront, contours of the change in pressure from the pre-interaction steady-state condition are plotted. Figure 5 shows the downstream development of the shock at time 0.45. The solid contour lines represent an increase in pressure, and dashed lines represent a decrease in pressure. A circular arc centered on the vortex core has been drawn in to emphasize the position of the wavefront. The dashed circular region corresponds to the decrease in pressure due to the vortex. It should be noted that the region of high pressure is developed at the point on the shock where the velocity induced by the vortex forces the shock to deflect downstream, thereby compressing the downstream flow. Similarly, the region of low pressure is developed at the point on the shock where the vortex pulls the shock upstream, thereby expanding the downstream flow.

In order to verify the acoustic nature of the wavefront, Fig. 6 shows a plot of radial distance of the wavefront from the vortex center against the time since the vortex center passed over the shock. It is seen that the wavefront is moving linearly with time. The slope of this line gives the speed of propagation of the wavefront, which in this case is found to be equal to the local speed of sound.

Although the results for the weak vortex-shock interaction are interesting because the development of an acoustic wave is predicted, they do not provide any information that cannot be obtained by using linear theory or other numerical techniques. The strength of the method presented here is in its ability to handle the interaction of a strong vortex with a shock. As the vortex strength is increased, the effect of the interaction on the shock is also substantially increased. The shock deflects more and when the vortex is strong enough, its impact with the shock causes not only deformation, but branching of the shock. When the interaction is this intense, the assumptions made in the linear theory are no longer valid an the implementation of shock-fitting techniques also becomes difficult. However, a shock capturing method of the type described in this paper is capable of predicting such interactions.

The results for the strong hybrid vortex, which corresponds to a normalized tangential velocity at the vortex core of 0.3, are presented in Fig. 7. This figure shows a time history of the pressure contours for the strong vortex-shock interaction. The time history is similar to that of the weak vortex interaction, until the normalized time of 0.25 when the vortex passes through the shock. The deflection of the shock is much more pronounced at this instant in time than it was for the weak vortex interaction. At time 0.35, it is apparent that the shock has branched into several shocks. The deformed shock structure shows the formation of two triple points. As time progresses, the branching of the shock becomes more pronounced. Figure 8 shows the change in density from the initial steady-state condition at a time of 0.45. This figure clearly shows the structure of the wavefront and the shockfront. Note that the two heavy lines in the figure represent the shock position before and after the interaction. The compression and expansion regions are seen to correspond to the locations of greatest excursion of the shock from the steady-state position.

Figure 9 shows the pressure distribution across the shock along the three lines AA′, BB′, and CC′, as shown in Fig. 7f. The relative strength of the newly formed shock structures is clearly represented in Fig. 9. Further, the pressure plots along lines AA' and CC' show that the total pressure increase across the shock takes place in two steps, whereas the pressure plot along line BB' shows that the entire pressure increase occurs in one single step. These pressure plots, therefore, confirm the formation of two triple points, due to the strong vortex-shock interaction.

The computed results described above are in good agreement with the experimental work of Naumann and Hermanns.[11] Figure 10 shows a Mach-Zehnder interferogram from the experimental strong vortex-shock interaction studies of Ref. 11. Also shown in Fig. 10 is a schematic of the experimentally observed features of the flow. It is seen that the vortex interaction with the shock has caused the shock to branch off into secondary shocks resulting in two triple points A and B. This is exactly what has been predicted by the present analysis and shown in Figs. 7-9.

The results obtained by the parametric studies provide information about the generation of sound in supersonic flows. Since the flow upstream of the shock is supersonic, the acoustic wave is limited to the region downstream of the shock. The sound wave is not generated until the vortex decelerates as it strikes the shock. This deceleration of the vortex is the same phenomenon that produces sound in subsonic flows. The sound wave created by the interaction process convects downstream with the vortex at the velocity of the downstream flow. The results also provide information about the physical nature of the acoustic wave. Referring back to Figs. 6 and 9, it can be seen that the acoustic wavefront has a distinctive high pressure, or compression region above the vortex core and upstream against the shock. There is also a definite expansion region below the vortex and upstream against the shock. The portion of the wavefront downstream of the vortex is not well defined, which implies that the strength of the wavefront is weaker in this region. This has been shown to be true in experiment and is also predicted in linear theory. In the early experimental studies of Hollingsworth and Richards, the portion of the wavefront ahead of the vortex was "ill-defined."[4] Furthermore, Ribner's linear theory predicts that for flows with an upstream Mach number of 1.1, the pressure fluctuations in the region downstream of the vortex core are an order

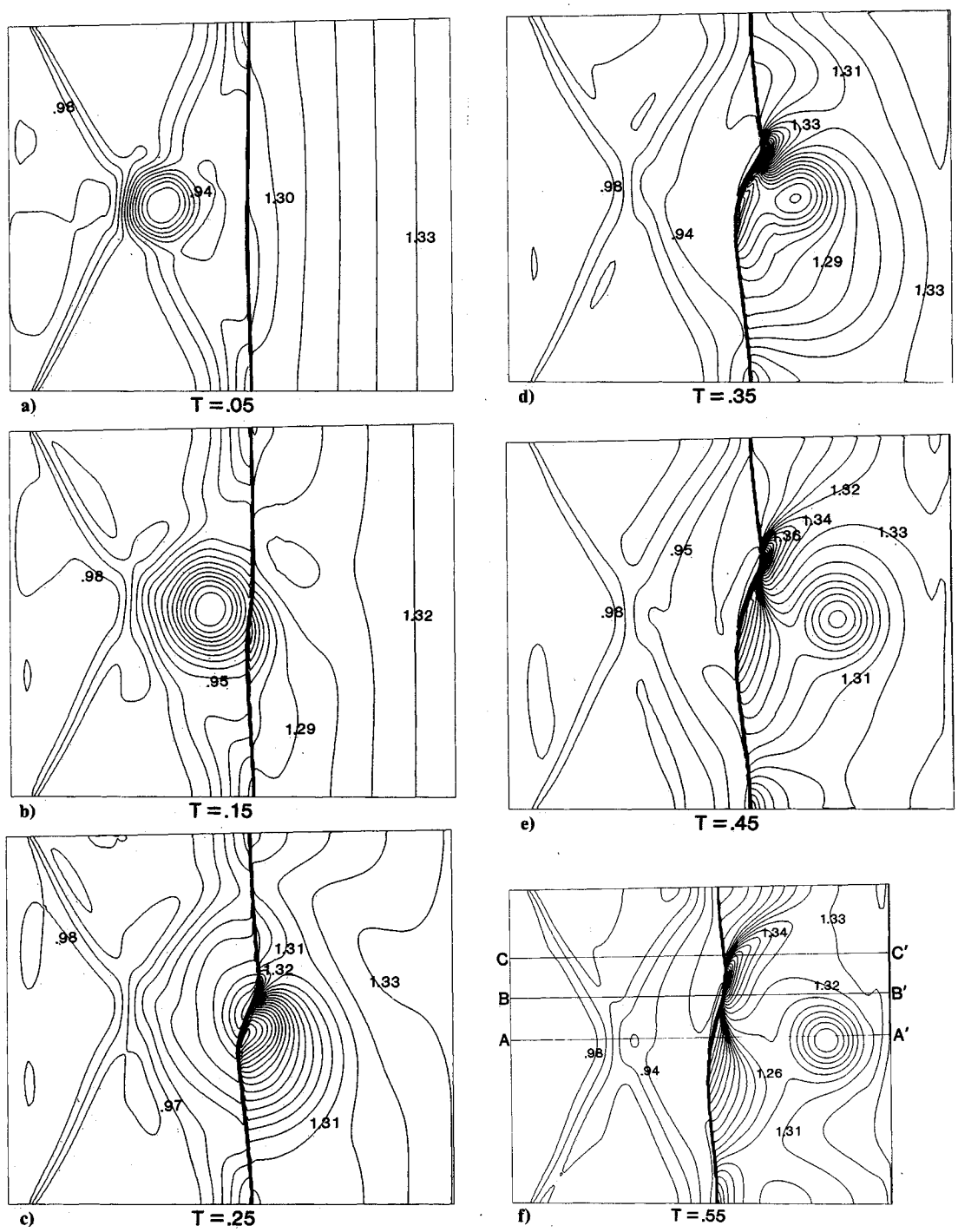

Fig. 7 Time history of pressure contours. Strong vortex ($U_c = 0.3$)

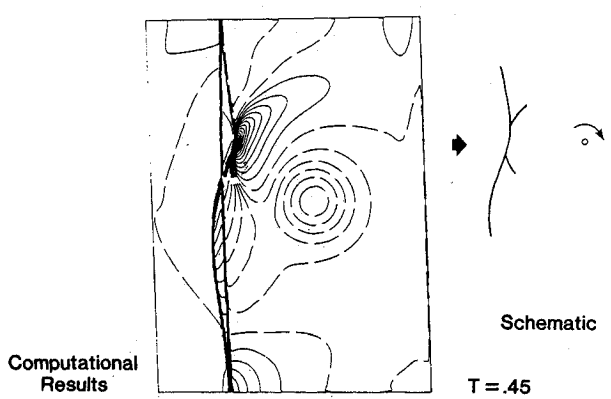

Fig. 8 Contours of change in density. Strong vortex ($U_c = 0.3$). Dashed lines represent loss in density from steady-state conditions. Solid lines represent increase in density.

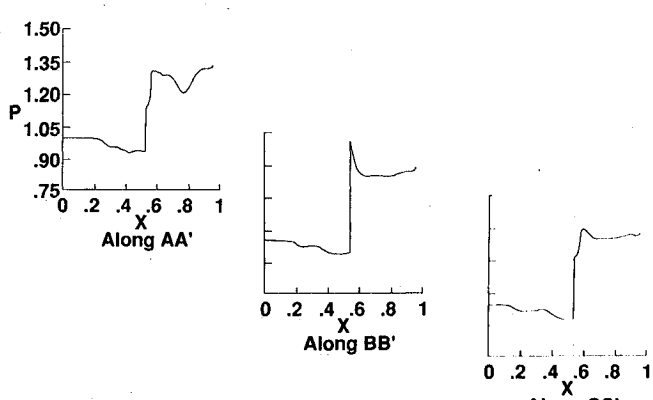

Fig. 9 Pressure distribution along locations AA′, BB′, and CC′, as marked on Fig. 7.

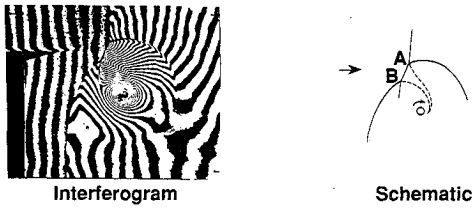

Fig. 10 Experimental study of strong shock-vortex interaction (from Ref. 11).

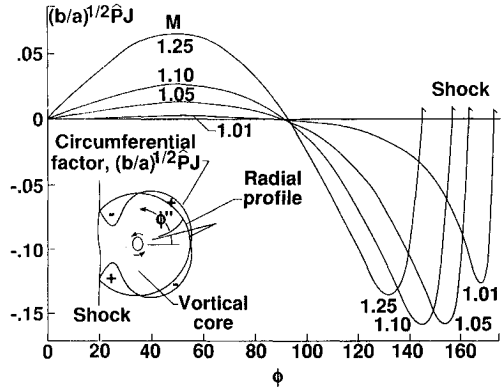

Fig. 11 Variation with ϕ'' of amplitude of normalized radial sound pressure profile at upstream $M = 1.01, 1.05, 1.1, 1.25$ (from Ref. 12).

of magnitude smaller than the fluctuations in the region closer to the shock (see Fig. 11).

Ribner's linear theory,[6,7] the experimental results of Dosanjh and Weeks,[9] and the numerical results of Pao and Salas[13] and Kopriva[17] indicate that the acoustic wavefront is quadrupole in nature. The experimental and numerical work performed by these authors was accomplished at higher Mach number flows than the work presented here. Studies are currently underway to determine if the acoustic wavefront can be more completely captured with this method for the more intense interaction at higher Mach number flows.

Concluding Remarks

A computational study of two dimensional shock-vortex interaction is described in this paper. A shock capturing second-order accurate upwind method is used to solve the Euler equations in conservation form. The results obtained in the study are encouraging in that some of the features of the shock-vortex interaction are captured properly. The computed flowfield and the associated acoustic field generated by the interaction agree qualitatively with the experimental results. Although the results presented here are encouraging, further work is required to more accurately predict the physics of such flows. Higher-order accurate methods, improved boundary conditions, and grid adaptation may be necessary to quantitatively predict the acoustic front and the pressure fluctuations associated with it. With these enhancements, the present approach to study the shock-vortex interaction problem will become much more robust than the approaches currently available in the literature and will be able to predict highly nonlinear interactions and cases of more practical significance. The present approach can also provide initial conditions for linear theory, so that propagation of the acoustic front into the far field can be predicted.

References

[1]Pao, S.P., and Seiner, J.M., "A Theoretical and Experimental Investigation of Shock-Associated Noise in Supersonic Jets," AIAA Paper 81-1973, Oct. 1981.

[2]Pao, S.P., and Seiner, J.M., "Shock-Associated Noise in Supersonic Jets," *AIAA Journal*, Vol. 21, No. 5, 1983, pp. 687–693.

[3]Moore, F.K., "Unsteady Oblique Interaction of a Shock Wave with a Plane Disturbance," NACA Rept. 1165, 1954.

[4]Hollingsworth, M.A., and Richards, E.J., "A Schlieren Study of the Interaction Between a Vortex and a Shock Wave in a Shock Tube," Aeronautical Research Council Rept. 17985, Fluid Motion Subcommittee 2323, London, 1955.

[5]Hollingsworth, M.A., and Richards, E.J., "On the Sound Generated by the Interaction of a Vortex and a Shock Wave," Aeronautical Research Council Rept. 18257, Fluid Motion Subcommittee 2371, London, 1956.

[6]Ribner, H.S., "Convection of a Pattern of Vorticity Through a Shock-Wave," NACA Rept. 1164, 1954.

[7]Ribner, H.S., "Shock-Turbulence Interaction and the Generation of Noise," NACA Rept. 1233, 1955.

[8]Ram, G.S., and Ribner, H.S., *The Sound Generated by Interaction of a Single Vortex with a Shock Wave*, Heat Transfer and Fluid Mechanics Institute, California Inst. of Technology, 1957, pp. 1–21.

[9]Dosanjh, D.S., and Weeks, T.M., "Interaction of a Starting Vortex as Well as a Vortex Street with a Traveling Shock Wave," *AIAA Journal*, Vol. 3, No. 2, 1965, pp. 216–223.

[10]Weeks, T.M., and Dosanjh, D.S., "Sound Generated by Shock Vortex Interaction," *AIAA Journal*, Vol. 5, No. 4, 1967, pp. 660–669.

[11]Naumann, A., and Hermanns, E., "On the Interaction Between a Shock Wave and a Vortex Field," AGARD-CP-131, 1973.

[12]Ribner, H.S., "Cylindrical Sound Wave Generated by Shock-Vortex Interaction," *AIAA Journal*, Vol. 23, No. 11, 1985, pp. 1708–1715.

[13]Pao, S.P., and Salas, M.D., "A Numerical Study of Two-Dimensional Shock-Vortex Interaction," AIAA Paper 81-1205, June 1981.

[14]Salas, M.D., Zang, T.A., and Hussaini, M.Y., "Shock Fitted Euler Solutions to Shock-Vortex Interations," *Proceedings of the 8th International Conference on Numerical Methods in Fluid Dynamics*, edited by E. Drause, Springer-Verlag, NY, 1982, pp. 461–467.

[15]Hussaini, M.Y., Kopriva, D.A., Salas, M.D., and Zang, T.A., "Spectral Methods for the Euler Equations: Part II, Chebyshev Methods and Shock Fitting," *AIAA Journal*, Vol. 23, No. 2, 1985, pp. 234–240.

[16]Kopriva, D.A., Zang, T.A., Salas, M.D., and Hussaini, M.Y., "Pseudospectral Solution of Two-Dimensional Gas Dynamic Problems," *Proceedings of 5th GAMM-Conf. on Numerical Methods in Fluid Mechanics*, edited by M. Pandolfi and R. Piva, Vieweg and Son, Braunschweig, Germany, 1983, pp. 185–192.

[17]Kopriva, D.A., "A Multidomain Spectral Collocation Computation of the Sound Generated by a Shock-Vortex Interaction," *Computational Acoustics: Algorithms and Applications*, Vol. 2, edited by D. Lee and M.H. Schultz, Elsevier Science Publishers B.V., Amsterdam, the Netherlands, IMACS, 1988.

[18]Anderson, W.K., and Thomas, J.L., "A Comparison of Finite Volume Flux Vector Splittings for the Euler Equations," AIAA Paper 85-0122, Jan. 1985.

[19]Thomas, J.L., Van Leer, B., and Walters, R.W., "Implicit Flux-Split Schemes for the Euler Equations," AIAA Paper 85-1680.

[20]Anderson, D.A., Tannehill, J.C., and Pletcher, R.H., *Computational Fluid Mechanics and Heat Transfer*, McGraw-Hill, NY, 1984.